Title
The BORDER family of negative transcription elongation factors regulates flowering time in Arabidopsis

Journal
Current Biology, 31(23)

ISSN
0960-9822

Authors
Yu, Xuhong
Martin, Pascal GP
Zhang, Yixiang
et al.

Publication Date
2021-12-01

DOI
10.1016/j.cub.2021.09.074

Peer reviewed

HHS Public Access

Author manuscript

Curr Biol. Author manuscript; available in PMC 2022 December 06.

Published in final edited form as:

Curr Biol. 2021 December 06; 31(23): 5377–5384.e5. doi:10.1016/j.cub.2021.09.074.

The BORDER family of negative transcription elongation factors regulate flowering time in Arabidopsis

Xuhong Yu[1,†,*], **Pascal G.P. Martin**[1,2,†], **Yixiang Zhang**[3], **Jonathan C. Trinidad**[3,4], **Feifei Xu**[5], **Jie Huang**[6], **Karen E Thum**[1,7], **Ke Li**[1], **ShuZhen Zhao**[8], **Yangnan Gu**[9], **Xingjun Wang**[8], **Scott D. Michaels**[1,*,#]

[1]Department of Biology, Indiana University, 915 East Third Street, Bloomington, IN 47405, USA.

[2]Current address, INRAE, Univ. Bordeaux, UMR BFP, 33882, Villenave d'Ornon, France

[3]Department of Chemistry, Indiana University, Bloomington, Indiana 47405, USA.

[4]Laboratory for Biological Mass Spectrometry, Department of Chemistry, Indiana University Bloomington, Bloomington, IN, USA.

[5]Institute of Nuclear Agricultural Sciences, Key Laboratory for Nuclear Agricultural Sciences of Zhejiang Province and Ministry of Agriculture and Rural Affairs, Zhejiang University, Zijingang Campus, Hangzhou 310058, China

[6]Center for Genomics and Bioinformatics, Indiana University, 915 East Third Street, Bloomington, IN 47405, USA.

[7]Current address, Stoller Enterprises, Houston, TX 77024.

[8]Shandong Provincial Key Laboratory of Crop Genetic Improvement, Ecology and Physiology, Biotechnology Research Center, Shandong Academy of Agricultural Sciences, Jinan, 250100, China.

[9]Department of Plant and Microbial Biology, University of California, Berkeley, CA, USA 94720

Summary:

Transcription initiation has long been considered a primary regulatory step in gene expression. Recent work, however, shows that downstream events, such as transcription elongation can also play important roles[1-3]. A well-characterized example from animals is promoter-proximal pausing, where transcriptionally engaged Pol II accumulates 30-50bp downstream of the transcription start

[*]Corresponding authors: xuhongy@gmail.com and michaels@indiana.edu.
[#]Lead contact
[†]Equal contribution

Author Contributions: X.Y., P.G.M., Y.G., X.W., F.X. and S.D.M. participated in the design of experiments. Y.Z. and J.C.T. performed mass spectrometry. X.Y., J.H., and P.G.M. created sequencing libraries and P.G.M. performed bioinformatic analyses. K.E.T, K.L., and S.Z. performed experiments. X.Y., P.G.M., and S.D.M. were responsible for writing and overall direction of the project.

Declaration of Interests: The authors declare no competing interests.

site (TSS) and is thought to enable rapid gene activation [2]. Plants do not make widespread use of promoter-proximal pausing, however, in a phenomenon known as 3′ pausing, a significant increase in Pol II is observed near the transcript end site (TES) of many genes[4-6]. Previous work has shown that 3′ pausing is promoted by the BORDER (BDR) family of negative transcription elongation factors. Here we show that BDR proteins play key roles in gene repression. Consistent with BDR proteins acting to slow or pause elongating Pol II, BDR-repressed genes are characterized by high levels of Pol II occupancy, yet low levels of mRNA. The BDR proteins physically interact with FPA [7], one of approximately two dozen genes collectively referred to as the autonomous floral-promotion pathway [8], which are necessary for the repression of the flowering time gene *FLOWERING LOCUS C (FLC)* [9-11]. In early-flowering strains, *FLC* expression is repressed by repressive histone modifications, such as histone H3 lysine 27 trimethylation (H3K27me3), thereby allowing the plants to flower early. These results suggest that the repression of transcription elongation by BDR proteins may allow for the temporary pausing of transcription or facilitate the long-term repression of genes by repressive histone modifications.

eTOC blurb

Yu *et al.* show that genes repressed by the BDR family of negative transcription elongation factors have high levels of Pol II occupancy, despite relatively low steady state RNA levels. In this way, BDR proteins may allow for the later resumption of transcription or facilitate the longterm repression of genes by repressive histone modifications.

Keywords

Transcription elongation; flowering time; RNA Polymerase II; pausing; *FLOWERING LOCUS C*; BORDER

RESULTS AND DISCUSSION

BDR proteins interact with autonomous pathway protein FPA

To investigate the molecular function of the autonomous pathway, we used yeast two-hybrid (Y2H) screens to identify binding partners of FPA [7,12]. Two related proteins, BDR1 and BDR2 were identified as FPA interactors in the library screen. BDR1 and BDR2 belong to a three-member protein family that also includes BDR3 [13]. Although BDR3 was not identified in the screen, all three proteins can interact with FPA in Y2H assays (Figure 1A). BDR proteins each contain a SPOC domain, which is found in the SPEN family of transcriptional repressors, and a TFIIS central domain (Figure 1C) [14,15]. Using truncated BDR proteins we found that the amino terminal region and TFIIS central domain are dispensable for the interaction with FPA (Figure 1B,C). In contrast, deletions that removed the SPOC domain or its N-terminal extension failed to interact. For BDR2, we also identified an alternatively spliced form (BDR2as) with a frame-shift that removes the SPOC and C-terminal domains (Figure 1A). This form did not interact with FPA (Figure 1A).

For BDR3, we found a one-base insertion relative to the reference TAIR10 assembly, creating a frame shift that extends the open reading frame by 145 amino acids, a sequence displaying homology to the C-terminal regions of BDR1 and BDR2. In Y2H assays full-

length BDR3 interacted with FPA but a truncated BDR3 corresponding to the current TAIR10 annotation failed to interact, consistent with the lack of interaction seen in the BDR2as clone (Figure 1A-C). Together, these results suggest that the C-terminal region of the BDR proteins is required for their interactions with FPA.

We used several approaches to verify that the interactions observed between FPA and BDR occur in plants. All three BDR proteins interact with FPA in bimolecular fluorescence complementation (BiFC) assays in tobacco cells, whereas the truncated BDR2as and BDR3t did not interact (Figure 1D). We also analyzed FPA-interacting proteins by immunoprecipitation - mass spectrometry (IP-MS) using an anti-FPA antibody to pull down proteins from wild-type Arabidopsis protein extracts or an *fpa* mutant as a control. In addition to FPA, we identified peptides corresponding to BDR1 (Table S1). Finally, in tobacco, a MYC-tagged version of FPA was able to co-immunoprecipitate HA-tagged versions of BDR1 and BDR2 (Figure 1E).

Like FPA, BDR proteins promote flowering by repressing *FLC* expression

FPA acts as an inhibitor of the floral repressor *FLC*, thus, *fpa* mutants are late flowering due to increased *FLC* expression [7,12]. Like FLC, BDR protein expression is highest in shoot and root apices (Figure S1A). To determine if BDR proteins also participate in the promotion of flowering, we examined the flowering time of *bdr* mutants. *bdr* single mutants did not show clear flowering-time phenotypes, however, the *bdr1,2,3* triple mutant showed a strong late-flowering phenotype (Figs. 2A, S1B). Amongst the double mutants, only *bdr1 bdr2* mutant showed a significant late-flowering phenotype, suggesting that *BDR1* and *BDR2* may play more significant roles in floral promotion than *BDR3*.

FLC transcripts levels are increased in *bdr1,2,3*, similar to levels seen in the *fpa* mutant (Figure 2C,D), suggesting that the late-flowering phenotype of *bdr* mutants is due to *FLC*. The late-flowering phenotype of autonomous-pathway mutants can be eliminated by loss-of-function mutations in *FLC* [16] or by a process known as vernalization, in which *FLC* is epigenetically silenced by H3K27 methylation following a prolonged cold exposure[9,10]. Consistent with BDR proteins acting as part of the autonomous pathway, the late-flowering phenotype of the *bdr1,2,3* triple mutant was eliminated by vernalization (Figure 2B) or in the *bdr1,2,3 flc* quadruple mutant (Figure 2E). In fact, the quadruple mutant flowered earlier than wild-type or the *flc* single mutant. This suggests that, in addition to promoting flowering by repressing *FLC*, the BDR proteins also act to repress flowering though an *FLC*-independent mechanism.

The autonomous pathway represses *FLC* by facilitating the deposition of repressive histone modifications. In particular, the autonomous pathway is required for Polycomb Repressive Complex 2 (PRC2) to deposit repressive histone H3 lysine 27 trimethylation (H3K27me3) at *FLC* chromatin [11]. In wild-type early-flowering strains of Arabidopsis, H3K27me3 is enriched in the body of *FLC* and gene expression is low. In autonomous-pathway mutants, H3K27me3 is strongly reduced and the activating H3K4me3 is enriched near the transcription start site, leading to increased *FLC* expression. To determine if the BDR proteins play a similar role in the repression of *FLC*, we examined the levels of H3K4me3 and H3K27me3 by Chromatin Immunoprecipitation (ChIP) followed by quantitative PCR

(qPCR). Consistent with previous studies [11], wild-type plants were enriched in H3K27me3 across the *FLC* locus and showed low H3K4me3 in the 5′ region (Figure 2F,G). The *bdr1,2,3* triple mutant and the autonomous-pathway mutants *fpa, ld,* and *flk* showed similar patterns of reduced levels of H3K27me3 and increased H3K4me3 (Figure 2F,G). Thus, like other members of the autonomous pathway, BDR proteins are required for the deposition of repressive histone modifications at *FLC*.

BDR proteins and FPA show overlapping chromatin localization and effects on transcription

To determine if BDR proteins and FPA have overlapping binding sites, we performed ChIP-seq using an antibody recognizing FPA. Consistent with its proposed role in 3′ end processing [17,18], FPA occupancy was highest just downstream of the TES (Figure 3A). Similar to BDR proteins[13], FPA binding was proportional to steady-state mRNA levels. To examine the correlation between FPA and BDR localization, we sorted genes by FPA level and generated heatmaps of BDR occupancy. At the 3′ ends of genes, there was a strong correlation of FPA and BDR protein occupancy (Figure 3C). Metaprofiles also showed peaks of FPA ChIP-seq signal at peaks of BDR1, BDR2 or BDR3 and vice versa (Figure S2A,B). Consistent with the correlation between FPA binding and mRNA levels, FPA occupancy was also correlated with Pol II occupancy (Figure 3C). Although FPA shows overlapping binding with the BDR proteins, FPA occupancy was largely unaffected in the *bdr1,2,3* mutant (Figure S2C). Thus, the BDR proteins are not required for the recruitment of FPA to chromatin. Overall, FPA and BDR proteins show overlapping patterns of chromatin localization, however, FPA has a strong preference for TES sites, whereas BDR1 and BDR2 are enriched at both TSS and TES regions[13].

We also found evidence for overlapping effects of BDR proteins and FPA on gene expression via RNA-seq. There was a significant overlap in genes with decreased or increased mRNA levels, in *bdr1,2,3* or *fpa* (Figure 3B, Table S2). The overlap was greatest, however, for activated genes. Amongst *bdr* single mutants, the *fpa* mutant was most similar to *bdr1* in terms of changes in mRNA levels (Figure 3D). We were unable to recover an *fpa bdr1,2,3* quadruple mutant, possibly due to lethality. Unlike BDR-activated genes, which preferentially have an upstream neighbor transcribed from the same strand[13], FPA-activated genes did not show a strong bias for the orientation of the upstream gene (Figure S2D). FPA-activated genes did, however, show a slight preference for having a downstream neighbor on the opposite strand (Figure S2D), suggesting that FPA may be important in regions containing converging TESs. This would be consistent with recent work showing that other autonomous pathway proteins, such as LD and FLD, play roles in the regulation of convergent genes[19].

BDR-repressed genes are characterized by high levels of Pol II occupancy, but low steady state mRNA levels

Given that BDR proteins prevent transcriptional interference by repressing Pol II elongation[13], we wondered if the repression of Pol II elongation might also help to explain the behavior of BDR-repressed genes. We determined Pol II occupancy by ChIP-seq in wild-type plants using antibodies recognizing Pol II, serine 5-phosphorylated Pol II (enriched in

initiation), or serine 2-phosporylated Pol II (associated with elongation) [20]. As expected, Pol II occupancy correlates well with mRNA levels (Figure 4A). The 5% of genes with the highest mRNA levels showed approximately four times higher Pol II signal than the average of all genes. As expected, non-expressed genes showed little Pol II binding.

We then examined Pol II occupancy at BDR-repressed genes. Compared to BDR-activated genes or non-differentially expressed (Not DE) control genes, BDR repressed genes had much higher Pol II occupancy in wild type (Figure 4A), nearly as high as the top 5% of genes with the highest mRNA levels. This result was unexpected as the mRNA levels of the top 5% is ~75 fold higher than the mRNA levels of BDR-repressed genes (Figure 4B). BDR-repressed genes also had significantly lower mRNA levels than BDR-activated genes (p=3e-41, Mann-Whitney test) or non-differentially expressed control genes (p=2e-26), despite having higher levels of Pol II on their gene bodies (Figure 4A,B). We also noted differences in the distribution of Pol II across the groups of genes. For the top 5% most highly expressed genes, the average of all genes, and non-DE controls, Pol II was relatively evenly distributed across gene bodies with a peak just after the annotated transcript end/polyadenylation site (TES) (Figure 4A, red arrow). BDR-repressed genes, in contrast, had lower Pol II occupancy in the 3′ portion of the gene, including the peak associated with 3′ pausing. To further investigate the role of BDR proteins in transcription elongation, we examined BDR-repressed genes in published 5′ GRO-seq and GRO-seq data sets[5]. Little difference was observed between BDR-repressed genes and controls in 5′ GRO-seq, suggesting comparable rates of initiation (Figure 4C,D). Consistent with our ChIP-seq data, GRO-seq shows a higher signal for BDR-repressed genes in gene bodies (Figure 4C). Taken together, these data are consistent with a model in which BDR proteins inhibit the progression of Pol II through the body of BDR-repressed genes, resulting in the accumulation of Pol II and possible premature PolII termination.

Histone modifications at BDR-repressed genes are more reflective of gene expression levels than Pol II levels

It is well established that specific post-translational histone modifications, such as H3K4 or H3K36 methylation, are deposited during transcription elongation via the physical interaction of Pol II with "epigenetic writers"[21]. The details of how these chromatin states are achieved is still an active area of research, but the process appears to be dependent on the recruitment of histone-modifying enzymes, transcription turn over, and Pol II transcription rate[22,23]. Given the high levels of Pol II, yet low levels of mRNA, observed from BDR-repressed genes, we wondered whether histone modifications at these genes would resemble those of actively expressed genes or repressed genes.

We used ChIP-seq to determine levels of histone modifications in wild-type plants (Figure 4E,S3A). A clear correlation was observed between mRNA levels and H3K4me3 and H3K36me3 for non-expressed genes, the average of all genes, and the genes in the top 5% for mRNA level (Figure 4E). Despite having higher Pol II occupancy than BDR-protected or non-differentially expressed genes (Figure 4A), BDR-repressed genes had much lower levels of H3K4me3 and H3K36me3 (Figure 4E). Thus, the chromatin state of BDR-repressed genes is better correlated with their relatively low mRNA levels than with their high Pol

II occupancy. Given the model that both the recruitment of Pol II-associated chromatin modifiers and repeated rounds of transcription are required for the effective deposition of histone modifications[23], our data suggests that transcription turn over may be the limiting factor in the deposition of H3K4me3 and H3K36me3 at BDR-repressed genes.

In the *bdr* mutant, Pol II decreases at BDR-repressed genes while mRNA levels increase

Taken together, the results above suggest that BDR proteins repress gene expression by impeding Pol II elongation, which leads to high Pol II occupancy at BDR-repressed genes. If this model is correct, more efficient transcription of BDR-repressed genes in the *bdr1,2,3* mutant may lead to higher mRNA levels, yet lower levels of Pol II occupancy. To test this hypothesis, we compared Pol II occupancy in wild type and *bdr1,2,3*. We sorted BDR-repressed genes, all of which show increased mRNA levels in the *bdr1,2,3* mutant, by BDR1 occupancy (Figure 4F). In wild type, a positive correlation was observed between BDR1 occupancy and Pol II occupancy, particularly for genes with the highest levels of BDR1 (Figure 4F,S3B). There was not a strong correlation between BDR1 and Pol II occupancy and mRNA level in wild type (Figure 4F) nor with the amplitude of change in mRNA level between bdr1,2,3 and wild-type. Consistent with our model, Pol II occupancy dropped at BDR-repressed genes in the *bdr1,2,3* mutant (Figure 4G,S3C). The decrease in Pol II was most pronounced in genes with the highest BDR1 occupancy, which are the most likely direct targets of BDR1. H3K4me3 and H3K36me3 also increased at these genes in the *bdr1,2,3* mutant, suggesting that increased transcription turn over may be important in establishing these modifications at BDR-repressed genes (Figure 4G,S3C). Overall, these data indicate that BDR proteins impede the efficient elongation by Pol II, leading to lower transcript accumulation and reduced accumulation of activating histone modifications.

In conclusion, this work supports a model in which BDR proteins repress gene expression by acting as negative transcription elongation factors. There are similarities and differences between promoter-proximal pausing in animals and the repression of gene expression by BDR proteins. Both mechanisms feature high Pol II occupancy within genes with low mRNA levels, but with different distributions along gene bodies. Promoter-proximal pausing involves NELF, which is absent in plants, and results in the accumulation of engaged Pol II at a discrete pausing site near the promoter [24]. BDR proteins, in contrast, promote a broad accumulation of paused or slow Pol II across the body of BDR-repressed genes. In animals, the release of promoter proximal pausing by P-TEFb is thought to provide a means of rapid and coordinated gene activation (e.g. heat shock genes in Drosophila) [25]. Additional investigation will be required to determine if BDR-mediated Pol II pausing might also serve as a means for the rapid activation of gene expression.

In addition to potentially allowing for future resumption of transcription, the repression of transcription elongation by BDR proteins could also facilitate the long-term repression of genes by repressive histone modifications. The deposition of H3K27me3 by PRC2 is inhibited by preexisting H3K4me3[26]. When genes are actively expressed, the repeated passage of Pol II and associated chromatin modifiers serves to reinforce the deposition of H3K4me3. By inhibiting the progression of Pol II, BDR proteins may provide an opportunity for the removal of H3K4me3 thus providing a suitable substrate for PRC2.

This may be the case for the repression of *FLC* by BDR proteins and the autonomous pathway. Both mathematical modeling and experimental investigations have shown that *FLC* regulation by the autonomous pathway is linked to coordinated changes in initiation, elongation rate, termination, antisense transcription, and chromatin modifications and architecture [18,27-29]. Although the precise order of events is still being elucidated, the repression of Pol II elongation by the BDR proteins may coordinate some of these molecular events at the *FLC* locus. For example, by inhibiting transcription cycles at *FLC*, BDR proteins could facilitate the removal of H3K4 methylation by the autonomous pathway histone demethylase FLD, enabling silencing by H3K27me3.

STAR METHODS

RESOURCE AVAILABILITY

Lead contact—Further information and requests for resources and reagents should be directed to and will be fulfilled by the lead contact, Scott Michaels (michaels@indiana.edu).

Materials Availability—All unique/stable reagents generated in this study are available from the Lead Contact without restriction.

Data and code availability

- The accession numbers for the transcriptome and ChIP-seq data reported in this paper are GEO: GSE112440, GSE112441, GSE113076, GSE113059, GSE113078, GSE131772.
- This paper does not report original code.
- Any additional information required to reanalyze the data reported in this paper is available from the lead contact upon request.

EXPERIMENTAL MODEL AND SUBJECT DETAILS

Arabidopsis thaliana was used in this study. All mutant and transgenic lines detailed in the Key resources table were in Col-0 background.

METHOD DETAILS

Plant growth conditions—*fpa-7, flk, ld-1, flc-3, brd1-1, brd2-1* and *brd3-1* have been described previously [13,31]. Seeds were surface sterilized with 70% ethanol for 10 minutes, plated on ¼ Murashige and Skoog medium, and stratified for 3 days at 4°C, to promote germination. Arabidopsis plants were grown in temperature-controlled rooms at 22°C in long days (16-h light/8-h dark) under cool-white fluorescent light with a light intensity of approximately 125 μmol m^{-2} s^{-1}. For vernalization treatment, imbibed seeds were cold treated for 30 days. Tobacco plants were grown in temperature-controlled rooms at 22°C in short days (8-h light/16-h dark) under cool-white fluorescent light with a light intensity of approximately 125 μmol m^{-2} s^{-1}.V

Constructs—cDNAs and genomic DNAs were amplified, cloned into pENTR/D-TOPO (Invitrogen), and confirmed by Sanger sequencing. For Y2H screening and pairwise

interaction assays, cDNAs with stop codons were transferred to pDEST32 and pDES22 using LR Clonase (Invitrogen) according to the manufacturer's instructions. For BiFC, cDNAs with stop codons were then transferred to pNYFP-X-gw and pCCFP-X-gw by LR reaction. BDR1-MYC, BDR2-MYC, and BDR3-MYC have been described previously [13].

Y2H—Full length FPA was used as a bait to screen a cDNA library prepared from vegetative shoot apices. Screening was performed by growing yeast on SC-Trp-Leu-His + 3AT (25 mM) plates and followed by X-gal assays. Pairwise interaction assays were carried out on SC-Trp-Leu-His +3AT or SC-Trp-Leu-Uracil plates.

BiFC—Proteins were fused with either the N-terminal portion of enhanced Yellow Fluorescent Protein (eYFP) or the C-terminal portion of enhanced Cyan Fluorescent Protein (eCFP) as described previously [32]. Constructs were transformed into *Agrobacterium tumefaciens* strain C58C1 [30] by electroporation. Agrobacteria with constructs were grown overnight (16 hrs) at 28°C and then resuspended at OD_{600nm} of 0.4 in 10 mM $MgCl_2$ and 100 μM acetosyringone (Sigma). The Agrobacteria suspensions were mixed in equal volume for transient transformation. Paired constructs were cotransformed into young leaves of 4-week-old tobacco plants. Infiltrated plants were grown for 48 hr under 8 hr light/16 hr dark conditions, then imaged using a Leica SP5 confocal microscope.

Co-immunoprecipitation and mass spectrometry—Nuclei were isolated from 3-day-old seedlings as described previously [44] Nuclei were resuspended in Extraction Buffer (50 mM Tris-HCl, pH 7.5, 150 mM NaCl, 5 mM MgCl2, 10% glycerol, 0.1% NP-40, 1 mM PMSF, 2 mM DTT and 1:300 Plant Protease Inhibitors (Sigma)) and were passed through a 27G ½ needle six times after being frozen and thawed three times. The nuclear extracts were centrifuged twice at 13000 rpm for 15 min at 4 °C and supernatants were transferred to new tubes. Immunoprecipitation was performed as described previously with minor modifications [45]. Briefly, the nuclear extracts were incubated with Agarose-protein A-bead-conjugated anti-FPA rabbit polyclonal antibodies, which were raised against C-terminal portion (536-901) of FPA protein (Covance), for 1 hour on a rotating platform. The complexes were then washed for 5 min with Extraction Buffer (8 times in total), resuspended in SDS loading buffer, and then boiled for 5 min before being resolved on 10% SDS PAGE gel. Gel strips were then subjected to LC-MS/MS.

For transient co-expression, FPA-MYC, BRD1-HA, BRD2-HA fusions were cloned into pTA7002 [33] and transformed into *Agrobacterium tumefaciens* strain C58C1 [30]. Paired constructs were cotransformed into young leaves of 4-week-old tobacco plants. Forty hours after infiltration, leaves were sprayed with 50 μM dexamethasone and harvested after 6 hours. Co-immunoprecipitation was performed as mentioned above. The immunocomplexes were resolved on 10% SDS-PAGE gel and transferred to nitrocellulose membrane for probing with anti-HA-peroxidase (Sigma) and then, after stripping the membrane, anti-c-Myc-peroxidase (Sigma). Signals were detected using SuperSignal West Pico Chemiluminescent Substrate (Thermo Scientific).

RNA expression analysis—Expression analysis was performed as described previously [13]. Briefly, RNA was isolated from 8-day-old seedlings using the Spectrum™ Plant Total

RNA kit (Sigma) and quantified with a NanoDrop 2000 Spectrophotometer. 3 μg of total RNA was reverse-transcribed into cDNA with Superscript™ III reverse transcriptase (Invitrogen) and 500 ng of oligodT primer. The resulting cDNAs were diluted 10-fold. 20 μl quantitative PCR reactions were performed using 10 μl Platinum SYBRR Green qPCR SuperMix-UDG kit (Invitrogen), 2 μl of diluted cDNA, 0.5 μl each primer (4 μM), 0.04 μl ROX reference dye, and 6.96 μl H2O. qPCR reactions were performed on a Mx3005P Real-Time PCR System (Agilent) (50°C for 2 mins, 95°C for 5 mins, 50 cycles of 95 °C, 5 secs, 60°C,20 secs, 72°C, 10 secs; 1 cycle of 95 °C 1 min, 55°C 30 secs, 95°C, 30 secs). Relative and absolute quantification were determined against the standard curves using MxPro QPCR software (the standard curves were made by sequentially diluting the synthesized cDNA four-fold until 1/1024; a no reverse transcriptase control was included as a negative control). *ACTIN 2* was used as a reference gene. The integrity of the final qPCR products was determined by melting curve analysis. The relative amount of *FLC* mRNA was normalized to the level of *ACTIN 2*[46]. All experiments were repeated at least three times with similar results.

RNA-seq—As detailed in GEO entry GSE112441, total RNA was extracted from three independent replicates of 8-day old seedlings from each genotype using Trizol reagent (Invitrogen) following the manufacturer's instructions. Libraries were prepared from 1.5μg of total RNA using Illumina TruSeq Stranded mRNA Library Prep kit. Libraries were sequenced on a NextSeq500 instrument at Indiana University Center for Genomics and Bioinformatics.

ChIP-qPCR—ChIP was performed as described previously [31]. Briefly, seeds were sown on Murashige and Skoog medium and stratified for 4 days at 4 °C. Whole 7-day-old seedlings grown under long-day conditions were harvested and fixed with 1% formaldehyde. Cross-linked samples were homogenized in lysis buffer (50 mM HEPES pH 7.5, 150 mM NaCl, 1 mM EDTA, 1% Trinton X-100, 0.1% sodium deoxycholate, 0.1% SDS, 2 mM DPDS, 1 mM PMSF, and 1:300 Plant Protease Inhibitors (Sigma)) and sheared by sonication. The homogenates were centrifuged twice at 13000 rpm for 15 min at 4 °C and the supernatants were transferred to new tubes. The supernatants were precleared with salmon sperm DNA/ protein A agarose slurry. The precleared samples were incubated with the antibodies against anti-H3K4me3 (17-614, Millipore) or H3K27me3 (07-449, Millipore). The protein A agarose/antibody/histone complexed were washed twice with Low Salt Immune Complex Wash buffer, once with High Salt Immune Complex Wash buffer, once with LiCl Immune Complex Wash buffer, and twice with TE Buffer. Precipitated DNA samples associated with modified Histone H3 were relatively and absolutely quantified with real-time PCR, similar to the RNA expression analysis (above) except using sonicated genomic input DNA to generate standard curves. Histone H3K4me3 and H3K27me3 enrichments at *FLC* locus were normalized against the *ACTIN 2*[46] locus. Data presented are an average of three replicates. Primers shown in Table S3.

ChIP-seq—Nuclei were isolated from cross-linked samples described as previously [47] and were then resuspended in nuclei lysis buffer (50mM Tris-HCl pH8, 10mM EDTA, 1% SDS, 1mM PMSF, 1% Plant Protease Inhibitors (Sigma)). After fragmentation using a Covaris

S200, the chromatin samples were diluted with ChIP dilution buffer (1.1% Triton X-100, 1.2mM EDTA, 16.7mM Tris-HCl pH8.0, 167mM NaCl, 1mM PMSF, 1% Plant Protease Inhibitors (Sigma)). Diluted chromatin samples were subjected to immunoprecipitation with antibodies (anti-FPA; anti-RNA polymerase II CTD repeat YSPTSPS antibody (8WG16), Abacm ab817; and control IgG Abcam ab18413) described as above.

Native histone ChIP was largely performed as described previously [48], with anti-Histone H3 Abcam ab1791, anti-Histone H3 (tri methyl K36) Abcam ab9050, anti-Histone H3 (tri methyl K4) Millipore 17-614, and anti-Histone H3 (di methyl K4) Millipore 17-677. ChIP libraries were prepared using NEBNext® Ultra™ DNA Library Prep kit (New England Biolabs) and sequenced on the NextSeq 500 platform at Center of Genomics and Bioinformatics, Indiana University.

Reanalysis of published datasets—In the present work, we used some sequencing datasets that we or other groups have previously published and that are publicly available from Gene Expression Omnibus (https://www.ncbi.nlm.nih.gov/geo/). Our RNA-seq data in *bdr* mutants (GSE112441), but not in the *fpa* mutant (also in GSE112441) was previously reported in [13]. An independent RNA-seq experiment is also available for *fpa* mutant in GSE112440. Our ChIP-seq data for BDR1, BDR2 and BDR3 (GSE113059 and GSE131772) were first reported in [13] and analyzed for gene sets distinct from those in the present article. Similarly, our Pol II ChIP-seq data (GSE113078) was previously analyzed [13] on other gene sets. Our ChIP-seq data for FPA (GSE113059) was not reported previously but was re-analyzed in [49] with a specific pipeline, different from the one used here and described in GSE11359. DNase hypersensitivity (DHS) data is from [50] and is available in GSE34318. DNAse-seq reads from the 3 replicates of wild-type seedlings were retrieved, trimmed with Trimmomatic 0.33 [40], remapped to TAIR10 using bowtie [51] allowing no mismatches (-v 0 -m 1 --strata --best) and merged in a single bam file. The reads were shifted to be centered on their 5′ ends before computing the coverage using R/bioconductor GenomicRanges functions [38]. GRO-seq and RNA-seq data from [5] (GSE83108) were trimmed with Trimmomatic 0.33 and reads longer than 20bp were remapped on TAIR10 using STAR 2.5.2b [34]. Uniquely mapped reads with a mapping quality >10 were selected using samtools 1.3.1 [35] to compute the strand-specific coverages using GenomicRanges functions.

Bioinformatic analyses—Raw and processed ChIP-seq and RNA-seq data, along with detailed experimental and bioinformatic procedures are provided in GEO Series GSE112443 and its subseries. TAIR10 annotations (www.arabidopsis.org) were used for all analyses. Blacklisted regions for ChIP-seq experiments were described previously[13].

RNA-seq computational analysis: RNA-seq data from GSE112440 were normalized as FPKM and used to define 9 groups of protein-coding genes differing by their average FPKM levels in 8 day-old Col-0 seedlings. The corresponding groups are provided as Table S1 in [13]. RNA-seq data from GSE112441 was used for differential expression analysis and all other analyses presented in this article. Paired-end reads (2x43bp) were mapped to TAIR10 genome using STAR v2.5.2b [34] with default parameters. Reads with mapping quality below 10 were removed using samtools 1.3.1 [35] and those uniquely mapping to TAIR10 annotated

genes were counted with featureCounts [36] from the Rsubread package 1.24.2 [37] of R 3.3.2 and Bioconductor 3.4 [38].

Analysis of differentially expressed protein-coding genes between wild-type Col-0 seedlings and single mutants for *bdr1, bdr2, bdr3, fpa* or *bdr1,2,3* triple mutant was done with DEseq2 1.14.1 [39]. A table of differentially expressed genes and corresponding statistics (logFC, raw p-value and adjusted p-value for all comparisons) is provided as Table S2. We also defined a set of 1408 control, non-differentially expressed genes ("Not DE") by selecting genes with high p-values ($p<0.45$) and low absolute log2(fold-change) (<0.25) for all comparisons (single *bdr1, bdr2, bdr3* and *fpa* mutants and the *bdr1,2,3* triple mutant vs wild-type) and removing genes with extreme read counts (DESeq2 basemean >3 and <1e5), as previously described [13].

ChIP-seq computational analysis: Adapter sequences were removed from paired-end reads using Trimmomatic 0.33 [40] and aligned to the Arabidopsis genome using Bowtie2 [41]. Duplicate fragments (Picard 2.2.4 MarkDuplicates) and low quality alignments (MapQ<2, samtools 1.3) were removed. For MNase-seq and ChIP-seq for histone modifications, fragment sizes between 70bp and 250bp were kept for analysis. Aligned reads were imported in R (v.3.3.2) to obtain coverages using Bioconductor v3.4 [52]. Coverages were normalized as fragments per 10 million fragments (FP10M) and exported to bigWig files with the rtracklayer package [42]. ChIP-seq peaks were detected using MACS2 2.1.0 [53] in paired-end mode. Peaks located in blacklisted regions were removed. Average profiles and metagene plots were produced as described in [13].

Multigene heatmaps: Multigene heatmaps were produced with the EnrichedHeatmap package [43] from coverages (in FP10M) that were averaged in 20bp bins before/after genomic features of interest (TSS, TES or peak center) or in bins covering every 1% of gene length along gene bodies. Changes in histone modification and Pol II were evaluated by calculating the difference between the binned coverage in *bdr1,2,3* mutant and the binned coverage in wild type before producing the heatmaps.

Quantification and Statistical Analysis

For flowering time analysis (Fig 2A,B, E) n=18 plants for each genotype. RT-qPCR (Fig 2C, D) and ChIP-qPCR (Fig 2G) data was acquired using MxPro-Mx3000P v4.10 QPCR SOFTWARE. The statistical test used, the p-value threshold, and the meaning of error bars are indicated in the legend of Figure 2. The significance of the intersection between genes regulated in *bdr1,2,3* and *fpa* (Fig 3B) was evaluated using Fisher exact test (fisher.test function in R 3.3.2) and the corresponding p-value is indicated in Fig 3B. As indicated in the legend of Fig 4, the differences in the expression of genes from the different groups shown in Fig 4B and 4D were evaluated by Wilcoxon rank sum test (R 3.3.2).

Supplementary Material

Refer to Web version on PubMed Central for supplementary material.

Acknowledgments

Next generation sequencing was performed at the Indiana University Center for Genomics and Bioinformatics. We thank Stephanie M DeYoung and Laurel B Bender for assistance with Y2H screening and antibody generation. We are grateful to the GenoToul bioinformatics platform Toulouse Midi-Pyrenees (Bioinfo GenoToul) for providing computing and storage resources. This work was supported by grants to S.D.M from the National Institutes of Health (GM075060), National Science Foundation (2001115) and the Indiana Clinical and Translational Sciences Institute and to Y.G. from the USDA National Institute of Food and Agriculture (CA-B-PLB-0243-H) and the National Science Foundation (2049931). PGM received the support of the EU in the framework of the Marie-Curie FP7 COFUND People Programme, through the award of an AgreenSkills+ fellowship (under grant agreement n°609398).

References

1. Adelman K, and Lis JT (2012). Promoter-proximal pausing of RNA polymerase II: emerging roles in metazoans. Nat Rev Genet 13, 720–731. [PubMed: 22986266]
2. Gaertner B, and Zeitlinger J (2014). RNA polymerase II pausing during development. Development 141, 1179–1183. [PubMed: 24595285]
3. Gilchrist DA, and Adelman K (2012). Coupling polymerase pausing and chromatin landscapes for precise regulation of transcription. Biochim Biophys Acta 1819, 700–706. [PubMed: 22406341]
4. Zhu J, Liu M, Liu X, and Dong Z (2018). RNA polymerase II activity revealed by GRO-seq and pNET-seq in Arabidopsis. Nat Plants.
5. Hetzel J, Duttke SH, Benner C, and Chory J (2016). Nascent RNA sequencing reveals distinct features in plant transcription. Proc Natl Acad Sci U S A 113, 12316–12321. [PubMed: 27729530]
6. Erhard KF Jr., Talbot JE, Deans NC, McClish AE, and Hollick JB (2015). Nascent transcription affected by RNA polymerase IV in Zea mays. Genetics 199, 1107–1125. [PubMed: 25653306]
7. Schomburg FM, Patton DA, Meinke DW, and Amasino RM (2001). FPA, a gene involved in floral induction in Arabidopsis, encodes a protein containing RNA-recognition motifs. Plant Cell 13, 1427–1436. [PubMed: 11402170]
8. Wu Z, Fang X, Zhu D, and Dean C (2020). Autonomous Pathway: FLOWERING LOCUS C Repression through an Antisense-Mediated Chromatin-Silencing Mechanism. Plant Physiol 182, 27–37. [PubMed: 31740502]
9. Michaels S, and Amasino R (1999). FLOWERING LOCUS C encodes a novel MADS domain protein that acts as a repressor of flowering. Plant Cell 11 (1040-4651), 949–956. [PubMed: 10330478]
10. Sheldon CC, Burn JE, Perez PP, Metzger J, Edwards JA, Peacock WJ, and Dennis ES (1999). The FLF MADS Box Gene. A repressor of flowering in Arabidopsis regulated by vernalization and methylation. Plant Cell 11, 445–458. [PubMed: 10072403]
11. Whittaker C, and Dean C (2017). The FLC Locus: A Platform for Discoveries in Epigenetics and Adaptation. Annu. Rev. Cell Dev. Biol 338, 1–8.
12. Meier C, Bouquin T, Nielsen ME, Raventos D, Mattsson O, Rocher A, Schomburg F, Amasino RM, and Mundy J (2001). Gibberellin response mutants identified by luciferase imaging. Plant J 25, 509–519. [PubMed: 11309141]
13. Yu X, Martin PGP, and Michaels SD (2019). BORDER proteins protect expression of neighboring genes by promoting 3' Pol II pausing in plants. Nat Commun 10, 4359. [PubMed: 31554790]
14. Chedin S, Riva M, Schultz P, Sentenac A, and Carles C (1998). The RNA cleavage activity of RNA polymerase III is mediated by an essential TFIIS-like subunit and is important for transcription termination. Genes Dev 12, 3857–3871. [PubMed: 9869639]
15. Ariyoshi M, and Schwabe JW (2003). A conserved structural motif reveals the essential transcriptional repression function of Spen proteins and their role in developmental signaling. Genes Dev 17, 1909–1920. [PubMed: 12897056]
16. Michaels SD, and Amasino RM (2001). Loss of FLOWERING LOCUS C activity eliminates the late-flowering phenotype of FRIGIDA and autonomous pathway mutations but not responsiveness to vernalization. Plant Cell 13, 935–941. [PubMed: 11283346]

17. Duc C, Sherstnev A, Cole C, Barton GJ, and Simpson GG (2013). Transcription Termination and Chimeric RNA Formation Controlled by Arabidopsis thaliana FPA. PLoS Genetics 9.
18. Sonmez C, Baurle I, Magusin A, Dreos R, Laubinger S, Weigel D, and Dean C (2011). RNA 3' processing functions of Arabidopsis FCA and FPA limit intergenic transcription. Proc Natl Acad Sci U S A 108, 8508–8513. [PubMed: 21536901]
19. Inagaki S, Takahashi M, Takashima K, Oya S, and Kakutani T (2021). Chromatin-based mechanisms to coordinate convergent overlapping transcription. Nat Plants 7, 295–302. [PubMed: 33649596]
20. Phatnani HP, and Greenleaf AL (2006). Phosphorylation and functions of the RNA polymerase II CTD. Genes Dev 20, 2922–2936. [PubMed: 17079683]
21. Smolle M, and Workman JL (2013). Transcription-associated histone modifications and cryptic transcription. Biochim Biophys Acta - Gene Regulatory Mechanisms.
22. Fong N, Saldi T, Sheridan RM, Cortazar MA, and Bentley DL (2017). RNA Pol II Dynamics Modulate Co-transcriptional Chromatin Modification, CTD Phosphorylation, and Transcriptional Direction. Mol Cell 66, 546–557.e543. [PubMed: 28506463]
23. Soares LM, He PC, Chun Y, Suh H, Kim TS, and Buratowski S (2017). Determinants of Histone H3K4 Methylation Patterns. Mol Cell. 68:773–785.e6. [PubMed: 29129639]
24. Levine M (2011). Paused RNA Polymerase II as a Developmental Checkpoint. Cell 145, 502–511. [PubMed: 21565610]
25. Fuda NJ, Ardehali MB, and Lis JT (2009). Defining mechanisms that regulate RNA polymerase II transcription in vivo. Nature 461, 186–192. [PubMed: 19741698]
26. Schmitges FW, Prusty AB, Faty M, Stutzer A, Lingaraju GM, Aiwazian J, Sack R, Hess D, Li L, Zhou S, et al. (2011). Histone Methylation by PRC2 Is Inhibited by Active Chromatin Marks. Mol Cell 42, 330–341. [PubMed: 21549310]
27. Fang X, Wu Z, Raitskin O, Webb K, Voigt P, Lu T, Howard M, and Dean C (2020). The 3' processing of antisense RNAs physically links to chromatin-based transcriptional control. Proc Natl Acad Sci U S A 117, 15316–15321. [PubMed: 32541063]
28. Jegu T, Latrasse D, Delarue M, Hirt H, Domenichini S, Ariel F, Crespi M, Bergounioux C, Raynaud C, and Benhamed M (2014). The BAF60 subunit of the SWI/SNF chromatin-remodeling complex directly controls the formation of a gene loop at FLOWERING LOCUS C in Arabidopsis. Plant Cell 26, 538–551. [PubMed: 24510722]
29. Wu Z, Ietswaart R, Liu F, Yang H, Howard M, and Dean C (2016). Quantitative regulation of FLC via coordinated transcriptional initiation and elongation. Proc Natl Acad Sci U S A 113, 218–223. [PubMed: 26699513]
30. Van Larebeke N, Engler G, Holsters M, Van den Elsacker S, Zaenen I, Schilperoort RA, and Schell J (1974). Large plasmid in Agrobacterium tumefaciens essential for crown gall-inducing ability. Nature 252, 169–170. [PubMed: 4419109]
31. Yu X, and Michaels SD (2010). The Arabidopsis Paf1c complex component CDC73 participates in the modification of FLOWERING LOCUS C chromatin. Plant Physiol 153, 1074–1084. [PubMed: 20463090]
32. Gampala SS, Kim TW, He JX, Tang W, Deng Z, Bai MY, Guan S, Lalonde S, Sun Y, Gendron JM, et al. (2007). An essential role for 14-3-3 proteins in brassinosteroid signal transduction in Arabidopsis. Dev Cell 13, 177–189. [PubMed: 17681130]
33. Xie Q, Frugis G, Colgan D, and Chua NH (2000). Arabidopsis NAC1 transduces auxin signal downstream of TIR1 to promote lateral root development. Genes Dev 14, 3024–3036. [PubMed: 11114891]
34. Dobin A, Davis CA, Schlesinger F, Drenkow J, Zaleski C, Jha S, Batut P, Chaisson M, and Gingeras TR (2013). STAR: ultrafast universal RNA-seq aligner. Bioinformatics 29, 15–21. [PubMed: 23104886]
35. Li H, Handsaker B, Wysoker A, Fennell T, Ruan J, Homer N, Marth G, Abecasis G, Durbin R, and Genome Project Data Processing, S. (2009). The Sequence Alignment/Map format and SAMtools. Bioinformatics 25, 2078–2079. [PubMed: 19505943]
36. Liao Y, Smyth GK, and Shi W (2014). featureCounts: an efficient general purpose program for assigning sequence reads to genomic features. Bioinformatics 30, 923–930. [PubMed: 24227677]

37. Liao Y, Smyth GK, and Shi W (2019). The R package Rsubread is easier, faster, cheaper and better for alignment and quantification of RNA sequencing reads. Nucleic Acids Res 47, e47. [PubMed: 30783653]
38. Lawrence M, Huber W, Pages H, Aboyoun P, Carlson M, Gentleman R, Morgan MT, and Carey VJ (2013). Software for computing and annotating genomic ranges. PLoS Comput. Biol 9, e1003118. [PubMed: 23950696]
39. Love MI, Huber W, and Anders S (2014). Moderated estimation of fold change and dispersion for RNA-seq data with DESeq2. Genome Biol 15, 550. [PubMed: 25516281]
40. Bolger AM, Lohse M, and Usadel B (2014). Trimmomatic: a flexible trimmer for Illumina sequence data. Bioinformatics 30, 2114–2120. [PubMed: 24695404]
41. Langmead B, and Salzberg SL (2012). Fast gapped-read alignment with Bowtie 2. Nat. Methods 9, 357–359. [PubMed: 22388286]
42. Lawrence M, Gentleman R, and Carey V (2009). rtracklayer: an R package for interfacing with genome browsers. Bioinformatics 25, 1841–1842. [PubMed: 19468054]
43. Gu Z, Eils R, Schlesner M, and Ishaque N (2018). EnrichedHeatmap: an R/Bioconductor package for comprehensive visualization of genomic signal associations. BMC genomics 19, 234. [PubMed: 29618320]
44. Cho YH, Yoo SD, and Sheen J (2006). Regulatory functions of nuclear hexokinase1 complex in glucose signaling. Cell 127, 579–589. [PubMed: 17081979]
45. Ream TS, Haag JR, Wierzbicki AT, Nicora CD, Norbeck AD, Zhu JK, Hagen G, Guilfoyle TJ, Pasa-Tolic L, and Pikaard CS (2009). Subunit compositions of the RNA-silencing enzymes Pol IV and Pol V reveal their origins as specialized forms of RNA polymerase II. Mol Cell 33, 192–203. [PubMed: 19110459]
46. Feys BJ, Moisan LJ, Newman MA, and Parker JE (2001). Direct interaction between the Arabidopsis disease resistance signaling proteins, EDS1 and PAD4. EMBO J 20, 5400–5411. [PubMed: 11574472]
47. Zemach A, Kim MY, Hsieh PH, Coleman-Derr D, Eshed-Williams L, Thao K, Harmer SL, and Zilberman D (2013). The Arabidopsis nucleosome remodeler DDM1 allows DNA methyltransferases to access H1-containing heterochromatin. Cell 153, 193–205. [PubMed: 23540698]
48. Bernatavichute YV, Zhang X, Cokus S, Pellegrini M, and Jacobsen SE (2008). Genome-wide association of histone H3 lysine nine methylation with CHG DNA methylation in Arabidopsis thaliana. PLoS ONE 3, e3156. [PubMed: 18776934]
49. Parker MT, Knop K, Zacharaki V, Sherwood AV, Tome D, Yu X, Martin PG, Beynon J, Michaels SD, Barton GJ, and Simpson GG (2021). Widespread premature transcription termination of Arabidopsis thaliana NLR genes by the spen protein FPA. Elife 10.
50. Zhang W, Zhang T, Wu Y, and Jiang J (2012). Genome-wide identification of regulatory DNA elements and protein-binding footprints using signatures of open chromatin in Arabidopsis. Plant Cell 24, 2719–2731. [PubMed: 22773751]
51. Langmead B, Trapnell C, Pop M, and Salzberg SL (2009). Ultrafast and memory-efficient alignment of short DNA sequences to the human genome. Genome Biol. 10, R25. [PubMed: 19261174]
52. Huber W, Carey VJ, Gentleman R, Anders S, Carlson M, Carvalho BS, Bravo HC, Davis S, Gatto L, Girke T, et al. (2015). Orchestrating high-throughput genomic analysis with Bioconductor. Nat. Methods 12, 115–121. [PubMed: 25633503]
53. Zhang Y, Liu T, Meyer CA, Eeckhoute J, Johnson DS, Bernstein BE, Nusbaum C, Myers RM, Brown M, Li W, and Liu XS (2008). Model-based analysis of ChIP-Seq (MACS). Genome Biol 9, R137. [PubMed: 18798982]

Highlights

- BDR proteins repress expression of the floral repressor, *FLC*
- BDR proteins physically interact with the autonomous pathway protein FPA
- BDR-repressed genes have high levels of Pol II occupancy, despite low mRNA levels
- Gene repression by BDR may involve the inhibition of transcription elongation

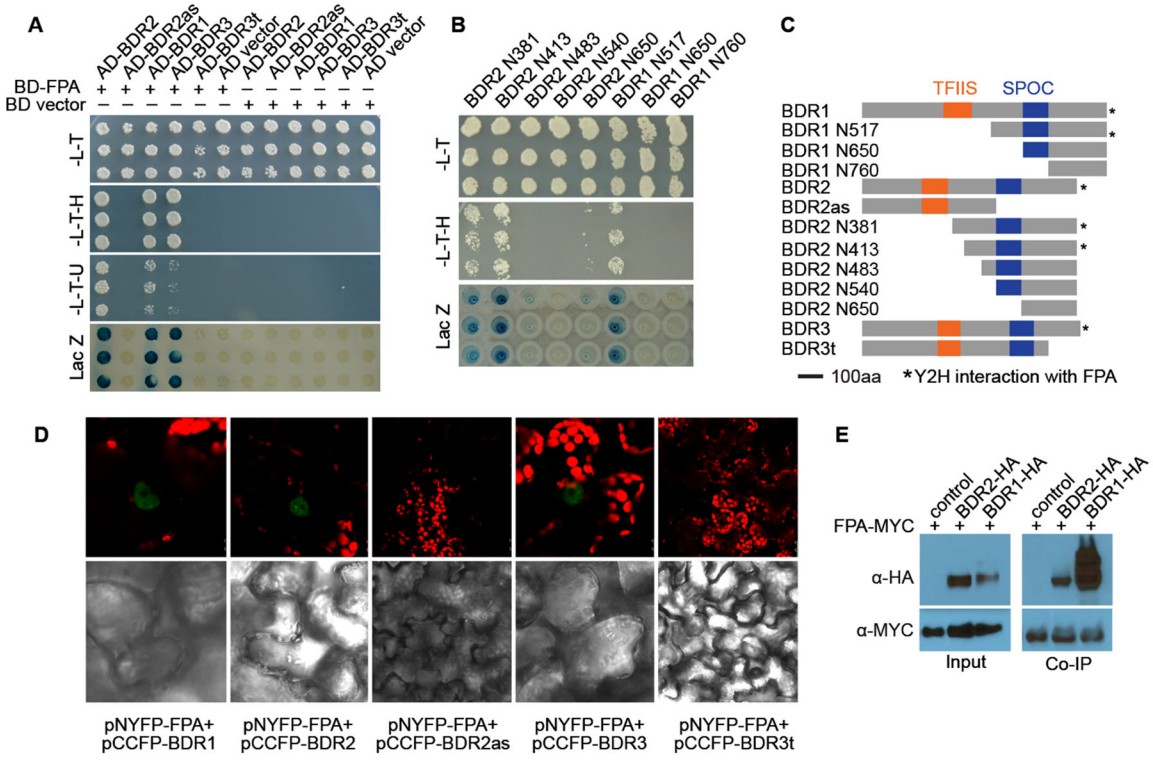

Figure 1. FPA physically interacts with BDR proteins.

A,B) Y2H interactions between FPA and BDR full-length and truncated proteins.

C) Schematic drawing showing full-length BDR proteins, variants, and deletion constructs.

D) BiFC interactions between FPA and BDR proteins. Chlorophyll autofluorescence appears in red and BiFC signal appears in green.

E) FPA pulls down BDR1 and BDR2 in co-IP assays performed using transient expression in tobacco.

See also Table S1.

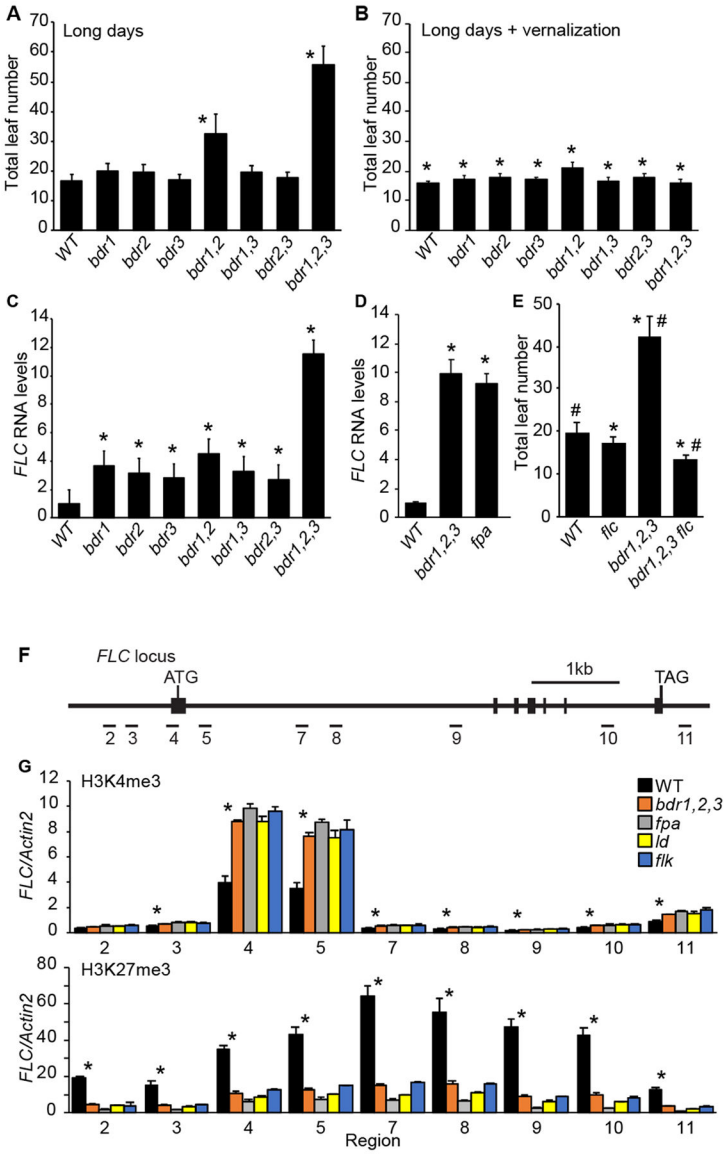

Figure 2. *bdr* mutants are late flowering and fail to repress *FLC*.

A) Flowering time of single and higher order *BDR* mutants.

B) The late-flowering phenotype of *bdr* mutants is eliminated by vernalization.

C) *bdr* mutations result in elevated *FLC* levels, as determined by qRT-PCR.

D) *FLC* levels in the *bdr1,2,3* triple mutant are similar to that found in *fpa*.

E) The late-flowering phenotype of *bdr1,2,3* is FLC-dependent.

F) Schematic drawing of the *FLC* locus. The location of primers used for qPCR are numbered.

G) ChIP-qPCR analysis of the *FLC* locus using antibodies recognizing H3K4me3 or H3K27me3.

Error bars indicate one standard deviation.

Asterisks indicate a significant difference from wild type (A,C-F) or non-vernalized samples (B).

# indicates a significant difference from *flc-3* (F). Asterisks indicate a significant difference between wild type and *bdr1,2,3*. Student's t-test, $p<0.01$.
See also Figure S1.

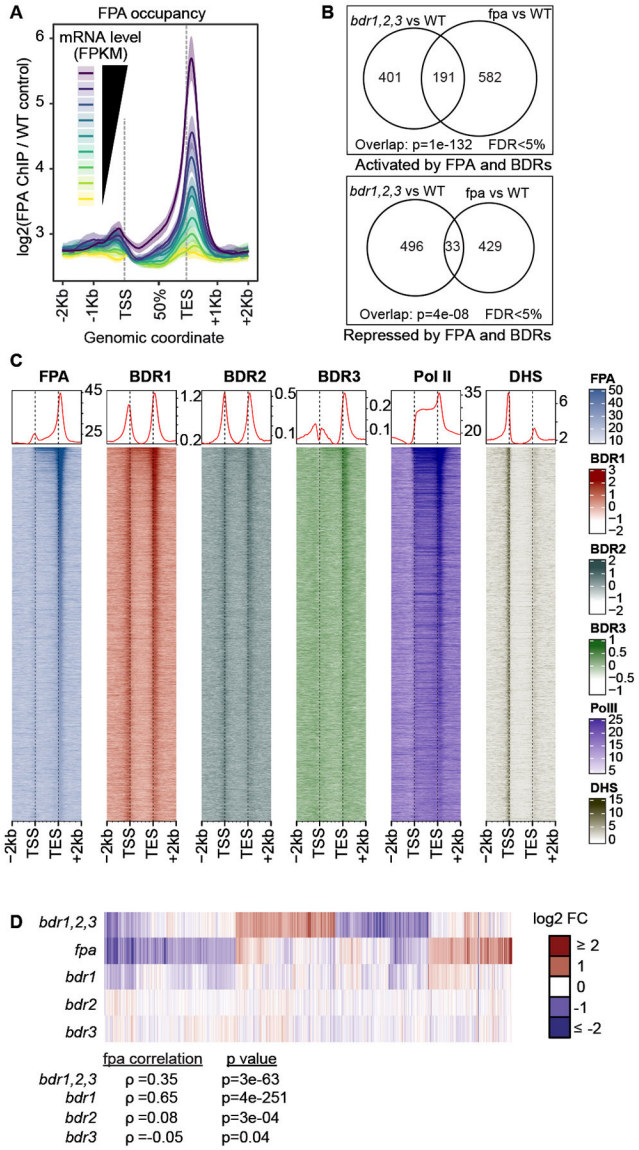

Figure 3. BDR proteins and FPA have overlapping localization and effects on expression.

A. Metagene profiles of FPA ChIP-seq signal in nine groups of genes defined by increasing mRNA expression levels in wild type (FPKM = fragments per kilobase per million aligned fragments). Average signal (line) and associated 95% confidence interval based on a Gaussian assumption (shade) are represented. Signal in gene bodies was averaged in bins of 1% of the gene size.

B. Venn diagram showing the overlap between genes activated or repressed by BDR proteins and FPA.

C. Heatmap and metagene profiles (top) of ChIP-seq signals and DNAse-hypersensitive sites (DHS). Genes were sorted by total FPA signal; the top 10,000 genes are shown.

D. Identification of BDR and FPA-regulated genes by RNA-seq analysis. Genes significantly regulated in at least one genotype are shown (FDR<5%). The Spearman rank correlation

coefficient and its significance evaluate the similarity of gene expression changes occurring in *bdr* mutants compared to *fpa* mutant.
See also Figure S2 and Table S2.

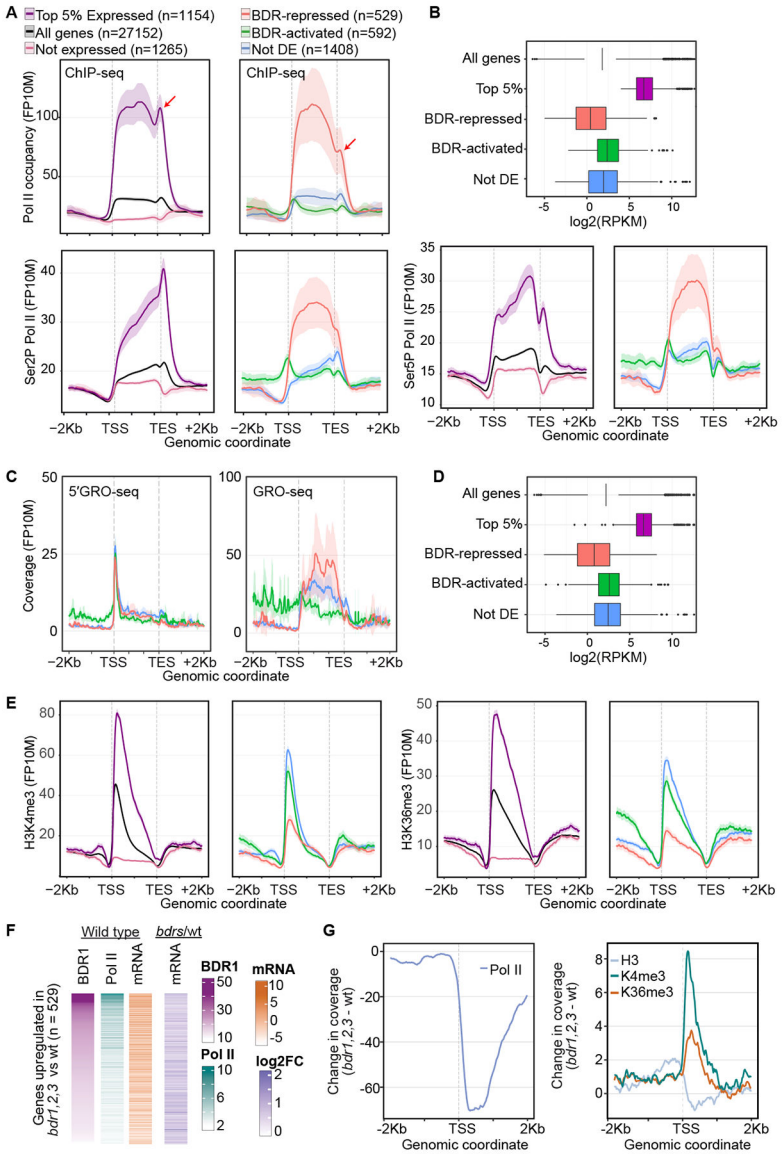

Figure 4. BDR-repressed genes have high Pol II occupancy, yet low levels of expression and signatures of repressed chromatin.

A, C. Metagene profiles of Pol II ChIP-seq (A), 5′GRO-seq, or GRO-seq coverage (C) across the indicated groups of genes in Arabidopsis seedlings. Red arrows indicate 3′ pausing.

B, D. Boxplots showing the mRNA levels for Pol II ChIP-seq (B) or 5′GRO-seq/GRO-seq (D) samples for the indicated gene classes. Differences are evaluated by Wilcoxon rank sum test.

E. Metagene profiles of histone modifications across the groups of genes indicated in (A).

F. BDR-repressed genes were sorted by BDR1 occupancy. Levels of BDR1, Pol II, and mRNA levels are shown for wild type. Also shown is the change in mRNA levels for BDR-repressed genes (*bdr1,2,3*/wt).

G. Plots showing the change in Pol II occupancy (*bdr1,2,3* - wt) and histone modifications around the TSS of BDR-repressed genes.

See also Figure S3.

KEY RESOURCES TABLE

REAGENT or RESOURCE	SOURCE	IDENTIFIER
Antibodies		
anti-HA-peroxidase	Sigma	H6533
anti-c-Myc-peroxidase	Sigma	16-213
anti-FPA	This study	N/A
anti-Histone H3	Abcam	ab1791
anti-Histone H3 (tri methyl K36)	Abcam	ab9050
anti-Histone H3 (tri methyl K4)	Millipore	17-614
anti-Histone H3 (di methyl K4)	Millipore	17-677
anti-Histone H3 (tri methyl K27)	Millipore	07-449
Bacterial and virus strains		
Agrobacterium tumefaciens C58C1	[30]	N/A
Escherichia coli TOP10	Invitrogen	C404010
Biological samples		
Chemicals, peptides, and recombinant proteins		
Plant Protease Inhibitors	Sigma	P9599
SuperSignal West Pico Chemiluminescent Substrate	Thermo	PI34580
Murashige and Skoog medium	VWR	IC2610024
Protein A agarose	Thermo	15918-014
Critical commercial assays		
NEBNext® Ultra™ DNA Library Prep kit	New England Biolabs	E7645S
Platinum SYBRR Greeen qPCR SuperMix-UDG kit	Thermo	11733038
Deposited data		
Gene expression profiling in wild-type, *fpa* mutant and *bdrs* triple mutant Arabidopsis seedlings	[13]	GSE112440
Gene expression profiling by RNA-seq of wild-type, *fpa* mutant, *bdr1* mutant, *bdr2* mutant, *bdr3* mutant and *bdrs* triple mutant Arabidopsis seedlings	[13]	GSE112441
Genome-wide profiling of nucleosomes (MNase-seq), total H3, H3K4me2, H3K4me3 and H3K36me3 (native ChIP-seq) in wild-type, *fpa* mutant and *bdrs* triple mutant	[13]	GSE113076
Genome-wide occupancy of BDR1, BDR2 and FPA (ChIP-seq)	[13]	GSE113059
Genome-wide profiling (ChIP-seq) of RNA polymerase II in wild-type, *fpa* mutant and *bdrs* triple mutant	[13]	GSE113078
Genome-wide occupancy of BDR1 and BDR3 (ChIP-seq)	[13]	GSE131772

REAGENT or RESOURCE	SOURCE	IDENTIFIER
Experimental models: Cell lines		
Experimental models: Organisms/strains		
Arabidopsis thaliana: Col-0	Widely distributed	N/A
Nicotiana benthamiana	Widely distributed	N/A
Arabidopsis: fpa-7	[31]	N/A
Arabidopsis: flk	[31]	N/A
Arabidopsis: ld-1	[31]	N/A
Arabidopsis: flc-3	[31]	N/A
Arabidopsis:bdr1-1	[13]	N/A
Arabidopsis:bdr2-1	[13]	N/A
Arabidopsis:bdr3-1	[13]	N/A
Arabidopsis:bdr1,2,3	[13]	N/A
Oligonucleotides		
See Table S3	This study	N/A
Recombinant DNA		
pENTR/D-TOPO	Invitrogen	K2400-20
pDEST22	Invitrogen	PQ1000101
pDEST32	Invitrogen	PQ1000101
pNYFP-X-gw	[32]	N/A
pCCFP-X-gw	[32]	N/A
BDR1-MYC	[13]	N/A
BDR2-MYC	[13]	N/A
BDR3-MYC	[13]	N/A
pDEST32-FPA	This study	N/A
pDEST22-BDR1	This study	N/A
pDEST22-BDR2	This study	N/A
pDEST22-BDR3	This study	N/A
pDEST22-BDR2as	This study	N/A
pDEST22-BDR3t	This study	N/A
pDEST22-BDR1 N517	This study	N/A
pDEST22-BDR1 N650	This study	N/A
pDEST22-BDR1 N760	This study	N/A
pDEST22-BDR2 N381	This study	N/A
pDEST22-BDR2 N413	This study	N/A
pDEST22-BDR2 N483	This study	N/A

REAGENT or RESOURCE	SOURCE	IDENTIFIER
pDEST22-BDR2 N540	This study	N/A
pDEST22-BDR2 N650	This study	N/A
pNYFP-FPA	This study	N/A
pCCFP-BDR1	This study	N/A
pCCFP-BDR2	This study	N/A
pCCFP-BDR3	This study	N/A
pCCFP-BDR2as	This study	N/A
pCCFP-BDR3t	This study	N/A
pTA7002	[33]	N/A
pTA7002-BDR1-HA	This study	N/A
pTA7002-BDR2-HA	This study	N/A
Software and algorithms		
STAR v2.5.2b	[34]	https://github.com/alexdobin/STAR
samtools 1.3.1	[35]	http://www.htslib.org/
featureCounts function from Rsubread package 1.24.2	[36]	https://www.bioconductor.org/packages/3.4/bioc/html/Rsubread.html
Rsubread package 1.24.2	[37]	https://www.bioconductor.org/packages/3.4/bioc/html/Rsubread.html
Bioconductor 3.4	[38]	https://www.bioconductor.org/packages/3.4
DEseq2 1.14.1	[39]	https://www.bioconductor.org/packages/3.4/bioc/html/DESeq2.html
Trimmomatic 0.33	[40]	http://www.usadellab.org/cms/?page=trimmomatic
Bowtie2	[41]	N/A
Picard 2.2.4 MarkDuplicates	Broad Institute	http://broadinstitute.github.io/picard/
rtracklayer	[42]	http://bowtie-bio.sourceforge.net/bowtie2/index.shtml
EnrichedHeatmap	[43]	https://www.bioconductor.org/packages/3.4/bioc/html/EnrichedHeatmap.html
GeneNeighborhood package v 1.0	Pascal GP Martin	https://github.com/pgpmartin/GeneNeighborhood
Scripts for ChIP-seq data analysis	Pascal GP Martin	https://github.com/pgpmartin/ChIPseq_functions
MxPro-Mx3000P v4.10	Agilent	N/A
Other		